

## BENDING CAPACITY OF PRECAST PRESTRESSED HOLLOW CORE SLABS WITH CONCRETE TOPPING

Izni S. Ibrahim<sup>1,\*</sup>, Kim S. Elliott<sup>2</sup> and Simon Copeland<sup>3</sup>

<sup>1</sup> Lecturer, Faculty of Civil Engineering, Universiti Teknologi Malaysia, 81310 UTM Skudai, Malaysia

<sup>2</sup> Associate Professor, School of Civil Engineering, University of Nottingham, University Park, Nottingham NG7 2RD, UK

<sup>3</sup> Technical Design Manager, Tarmac Topfloor Limited, Weston Underwood, Ashbourne, Derbyshire DE6 4PH, UK

Corresponding author: [Iznishahrizal@utm.my](mailto:Iznishahrizal@utm.my)

---

**Abstract:** This paper presents the effect of surface roughness (smooth and rough) and surface condition (ponded and optimum wet) on the bending capacity of precast prestressed hollow core slabs with in-situ concrete toppings by a series of full-scale experimental tests. Interface slip was also measured throughout the test to observe the composite behaviour of the test specimens. The tests result show that the ultimate bending capacity for the ponded condition for the smooth and rough surfaces was 3 to 5% less than that of the optimum wet even though they were still higher than the calculated values. A slip of 0.08 mm was observed for the smooth-ponded specimen. It was later found that by roughening the top surface of the precast prestressed hollow core slab, full composite action can be achieved if the interface slip is reduced or eliminated. A theoretical method to predict the deflection with partial interaction is also presented in this paper based on the experimental strain gradient. From the theoretical approach, the findings suggest that an interface slip still may had occurred near the mid-span region although it was not detected by the slip gauge located at both ends of the specimen.

**Keywords:** *Hollow core slabs; In-situ concrete toppings; Composite action; Bending capacity; Interface slip*

### 1.0 Introduction

Precast concrete flooring offers an economic and versatile solution to ground and suspended floors in any type of building construction. There is a wide range of precast flooring types available to give the most economic solution for all loadings and spans which includes hollow core slab (HCU), double-tee slab, solid composite plank and beam & composite plank. Cast in-situ concrete toppings are added to precast slab for the

purpose of making a complete floor finish, or to enhance the structural performance of the floor by producing a composite structure (Fig. 1). The in-situ concrete toppings are usually 40 to 100 mm in thickness, and contain a small amount of steel reinforcement (usually a prefabricated welded mesh) to control shrinkage. The concrete toppings would be laid in all weather conditions onto aged HCU of unspecified surface characteristics. The concrete toppings compressive strength usually varies between 25 and 40 N/mm<sup>2</sup> and lay onto repeated HCUs manufactured using semi-dry high strength concrete. Each year the UK industry constructs around £30m of composite hollow core floors slabs with no bona fide information about their design, surface preparation and construction. Relative movement between the wet cast concrete toppings on the HCU, and the injudicial placement of mesh reinforcement and construction joints, causes delamination, edge restraint, curvature and loss of serviceability. This is illustrated in Fig. 2. Ultimate failure modes could be brittle, especially on precast prestressed floors that have a high strength-stiffness ratio. Costly remedial work, lost utilities during repair and reduced thickness of concrete toppings could save about €25 – 35 million per year in Europe alone (based on about 2% of concrete toppings requiring attention) (Elliott 2002).

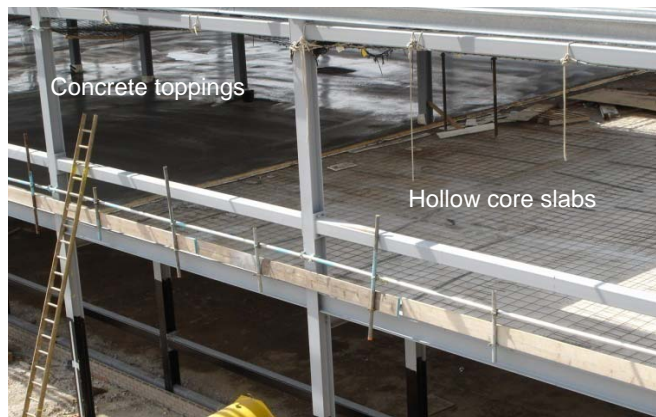


Figure 1 Concrete toppings on hollow core slabs

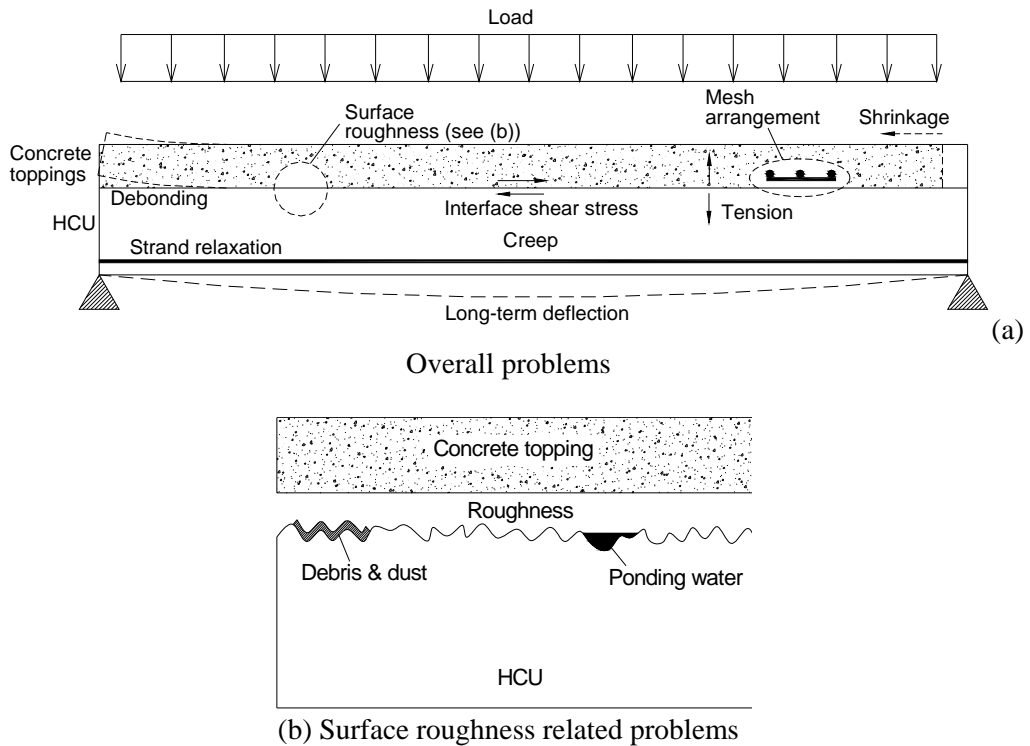


Figure 2 Problems related to concrete toppings construction

Improper surface preparations and construction techniques causes problems to the overall structural behaviour when cast in a monolithic manner. The contractor often neglected the effect of moisture content, shrinkage or surface characteristics of the HCU during concrete topping construction. Some attempts to quantify surface texture are given in the Fédération Internationale de la Précontrainte (FIP) document on interface shear in composite floor structures. The topping must be continuously reinforced, ideally at mid-depth, and as welded fabric is the preferred choice, there are problems where 3 or 4 sheets are lapped. Delays of up to 5 days can also accrue by not knowing when the conditions are right for laying. The research aims are to study the effects of surface preparation in terms of (i) roughness (smooth (as-cast) and roughened), (ii) pre-soaking before the casting of concrete toppings (ponded and optimum wet = approximately 9.5 litres/m<sup>2</sup> until the surface was light dark grey in colour).

## 2.0 Background Problems and Related Works

A composite member is designed to act monolithically. Nevertheless, as the member is bent in flexure, the HCU and the in-situ concrete topping tend to slide relative to each

other as shown in Fig. 3. Horizontal shear transfer along the interface between the HCU and the in-situ concrete topping is an essential requirement to ensure composite action of the two members.

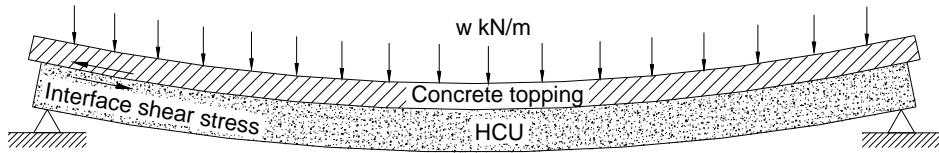


Figure 3 Horizontal shear stress along the interface of a composite member bent in flexure

When in-situ concrete is cast on a precast unit there is usually no mechanical key in the form of reinforcement provided between the two types of concrete. Reliance has to be made on the bond and shear strength between the contact surfaces. In the FIP Guide to Good Practice (FIP 1982), the types of surface which a precast unit may have, prior to receiving the in-situ concrete are identified into ten categories. They were categorised based on the end production of the precast unit and it is difficult to distinguish between “smooth” and “rough” surface. Within the FIP Commission itself there is a popular theory that smooth (clean) interfaces have better overall bond than roughened (often dusty and dirty) surfaces where localised bond failures occur. FIP (FIP 1982) recommends that contaminants should be removed either by water flushing, compressed air or vacuum cleaning. Sweeping is not sufficient as the small depressions of the interface will become full of dust. Other than roughness, surface treatment plays a major role with regard to the transfer of shear stress across the interfaces because:

- (a) Laitance skin, dust, debris, water etc. are commonly found in the crevices of the surface, where, as the tops tend to be less affected; the rougher the surface, the less susceptible it is to the quality of workmanship in cleaning and preparation.
- (b) If the surface of the precast member, before casting, is very dry, this member will absorb water from the in-situ concrete, so that the quality adjacent to the interface is governing for the capacity of the interface.
- (c) If the surface is very wet, i.e. ponded, the water-cement ratio at the interface will be very high, resulting in weak bond strength in the immediate strata.

When the surface pores are full treated, it is said to be surface-dry and saturated (wet conditions). If the precast surface was left to stand free in dry air before the casting of concrete toppings, some of the water contained in the unit will evaporate and be less than saturated, i.e. air dry (dry conditions). To produce a bone-dry surface condition, prolonged drying in an oven or in a closed hot compound would reduce the moisture content in the concrete until no moisture is left. However, this condition is not achievable for large scale production of precast units and is not considered in this study. The various stages of surface conditions are shown in Fig. 4. For an extreme condition, surface

moisture is left ponding, making it saturated and moist (ponded conditions). Walraven (Walraven 1991) stated that if the surface of the precast unit before casting is very dry it will absorb water from the concrete toppings, where the quality adjacent to the interface is governed by the capacity of the interface. In contrast, if the surface was ponded the large amount of free water on the surface will weaken the bond at the interface, thus reducing the capacity of the composite slab.

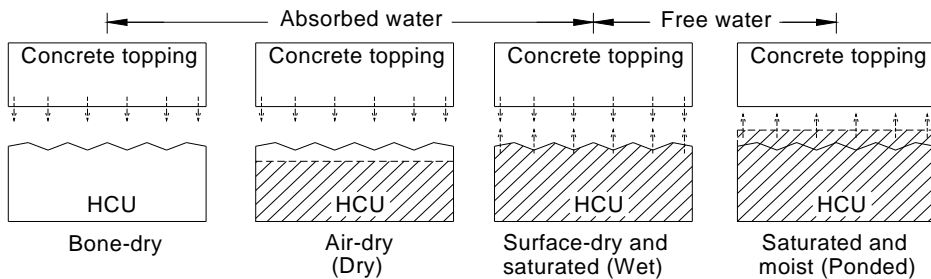


Figure 4 Conditions at the interface with different types of surface preparation

Tests carried out by Scott (Scott 1973), Ros (Ros, Cabo et al. 1994), Ueda & Stitmannathum (Ueda and Stitmannathum 1991) and Girhammar & Pajari (Girhammar and Pajari 2008) on HCU with concrete toppings were to ensure monolithic behaviour up to the ultimate loading capacity. The bond between hollow core slabs and the topping is essential and therefore it has to be checked in design and ensured in construction. The test parameters include surface roughness, load transmission between a group of two slabs, pre-stressing force, tension reinforcement ratio, shear span-to-effective depth ratio and concrete topping depth. In 2007, a more extensive work was carried out by Ajdukiewicz et al. (Ajdukiewicz, Kliszczewicz et al. 2007) with two different test setup; (i) short-term loading subjected to instantaneous bending tests until failure and (ii) 6 months long-term loading followed by ultimate bending tests until failure. The same conclusion was made by these researchers where the cracking and ultimate load increased between 10 and 42% compared to the HCU alone. Although there was an improvement to the ultimate load, there is still some lack of information on the surface condition during casting, the degree of roughness and interface slip which plays a major role to the overall performance of the composite slab. These parameters is studied in detail using full-scale test and presented in this paper.

### 3.0 Test Specimen and Experimental Setup

Precast slabs with circular hollow cores of constant 72 mm diameter, 1200 mm in width and 6300 mm in length were made. The units were pre-tensioned with nine number 7-wire helical strands of 9.3 mm and 12.5 mm diameter, placed with a 40 mm bottom cover. They were pre-tensioned to 70% of the ultimate strength,  $f_{pu} = 1770 \text{ N/mm}^2$  before

the concrete was cast. The maximum aggregate size was 10 mm and 20 mm for the unit and concrete toppings, respectively. The length and strands arrangement produces design service and ultimate bending moments of 53.59 kNm and 89.01 kNm, respectively. The HCU concrete compressive cube strength was 85.5 N/mm<sup>2</sup> at 28 days based on the average of 3 cubes of 100 × 100 × 100 mm dimension. Two types of surface finishes were studied; (i) rough (by raking the top surface with a stiff brush in the transverse direction), and (ii) smooth (as-cast).

The concrete toppings depth was 75 mm over a length of 6 m, leaving 150 mm at each end in order to measure interface slip. The concrete topping compressive strength was designed to achieve 30 N/mm<sup>2</sup> at 7 days. The concrete topping properties during the test day are given in Table 1. A142 (R6–200 mm) prefabricated mesh with 25 mm cover were laid on top of the HCU to increase the flexural strength and also to distribute the flexural cracks into the shear span. All sheets were adequately lapped at 300 mm in the mid-span region. The overall nominal geometry of the specimens and test layout are illustrated in Fig. 5 and 6, respectively. A three load cyclic test was applied and removed incrementally before the final load was applied until failure. The testing procedure follows that specified in BS 8110: Part 2 (BSI 1985). The cyclic load was applied until the calculated cracking moment,  $M_{crack\ calc}$  was attained (see Fig. 8). At the end of each cycle, the prestressed recovery was determined during 1 hour and 24 hours recovery period from the measured mid-span deflection at the end of the time period. The rate of loading was kept constant at 10 kN/min (or bending stress of 0.02 N/mm<sup>2</sup>/sec).

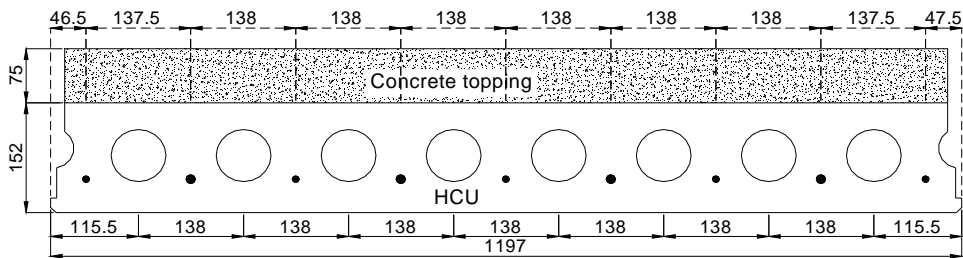


Figure 5 Specimen section and detailed dimension for the bending test  
(all dimensions are in mm)

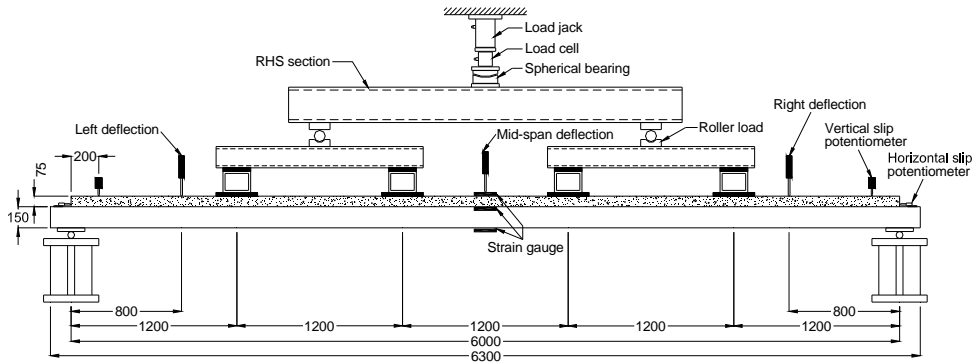


Figure 6 Bending test setup (all dimensions are in mm)

Table 1 Concrete topping properties

Specimen	Surface roughness	Surface condition	Concrete cube compressive strength (N/mm <sup>2</sup> )	Elastic Modulus (kN/mm <sup>2</sup> )	Cylinder splitting strength (N/mm <sup>2</sup> )	Flexural strength (N/mm <sup>2</sup> )
SS1	Smooth	Ponded	35.2	29.2	2.82	3.47
SS2		Optimum wet	30.8	28.1	2.64	3.27
SR1	Rough	Ponded	36.5	30.7	2.95	3.62
SR2		Optimum wet	37.3	28.8	2.98	3.65

*Note: Average of 3 tests*

#### 4.0 Surface Roughness and Surface Condition

Roughness was measured using an instrument developed by Bensalem (Bensalem 2001) as shown in Fig. 7. The instrument is placed on top of the slab to measure the roughness along a sampling length of 200 mm. Once the instrument is in place, the slider moves freely without displacing the instrument itself. Roughness was measured at three locations in the longitudinal direction; mid-span, left and right end of the HCU. The average was taken of the three measured locations.

Two different types of surfaces were prepared before casting the concrete topping, i.e. optimum wet and ponded. The prepared condition was based on the results of

the “push-off” test where the ponded was the least value in terms of interface shear strength (Ibrahim and Elliott 2006). The optimum wet was the preferred condition as mentioned in the FIP document (FIP 1982) with the HCU being light dark grey in colour with no standing surface water. Compared to being wet, ponded means excess water was purposely left on the surface with a depth of approximately 1.8 mm. Preliminary studies were also carried out to produce the optimum wet and ponded conditions on a 1 m × 1 m surface area. The time required for the water to evaporate was measured and for the surface to change to the light dark grey in colour for the optimum wet, in contrast to the ponded condition. The preliminary studies show that for ponded surface conditions, it requires 45 litres/m<sup>2</sup> of water as compared with the optimum wet surface which only requires 9.5 litres/m<sup>2</sup> of water. Another method of measurement was also carried out using a moisture meter (given in percentages). For the ponded condition, the surface moisture was between 41 and 43% and the optimum wet was between 26 and 28% without any standing water on the surface. All the results from the preliminary studies were then used as guidance to prepare the required surface conditions.

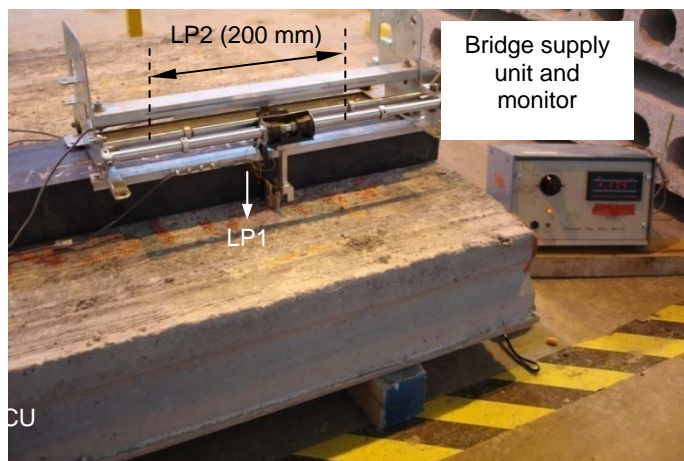


Figure 7 Surface roughness instrumentation

## 5.0 Experimental Results

### 5.1 Bending Moment and Deflection Relationship

The bending moment and mid-span deflection relationships are shown in Fig. 8. Deflections recorded at 0.8 m from the left and right supports were the same, proving that the loading and test rig position was centrally aligned throughout the test. During the

cyclic load test up to  $M_{sr\ calc}$ , the deflection was within the limit of  $\frac{L}{250} = 24\text{ mm}$ . The  $M_{sr\ calc}$  was calculated at two stages of loading – Stages 1 and 2 before and after hardening

of concrete topping as described by Elliott (Elliott 2002). This shows that all specimens were behaving elastically before cracking first occurred. Cracking occurred in specimen SR1 and SR2 during the first cyclic load increment at 107.7 and 119.8 kNm, respectively. It was also observed that for specimen SR1, the first crack occurred below the calculated  $M_{crack\ calc}$  (Elliott 2002). The prestressed recovery results for each loading cycle are given in Table 2. The recovery was consistent between 80 and 84% in the 1<sup>st</sup> and 2<sup>nd</sup> cycle. In the 3<sup>rd</sup> cycle, the recovery dropped below 80% for all specimens. The results found that the recovery for all specimens was less than the required 85% recovery for prestressed Class 1 and 2 category stated in BS 8110: Part 2 (BSI 1985). The reason for the low percentage recovery was because the load applied was more than the service load. This was taken into consideration since BS 8110: Part 2 (BSI 1985) stated that if the measured deflection is very small (e.g. span/1000), estimates of recovery become meaningless. This means that the measured deflection must be more than 6 mm in order to comply with the code requirement. In addition, specimen SR1 and SR2 had developed flexural cracks during the load increment, which had affected the specimen recovery.

The experimental curves at elastic or before reaching  $M_{crack\ calc}$  follow the calculated deflection for the uncracked section,  $EI_u$ . The ultimate bending moment capacity for specimen SS1 and SR1 were 190.3 and 178.2 kNm, respectively, which were 4.4 to 9.5% lower than specimen SS2 (196.8 kNm) and SR2 (188.1 kNm). These were the ponded condition specimens with smooth and rough surfaces, respectively. This is a possible explanation of the excess water that was not removed during the casting of the concrete toppings, which reduced the ultimate bending moment capacity compared to the optimum wet. However, the results were still higher than  $M_{ur\ calc}$  (see Table 2). The  $M_{ur\ calc}$  was also calculated using the two-stage approach rather than the one-step approach which is obviously less conservative. The method is to calculate the area of steel,  $A_{ps1}$  required in Stage 1, and to add the area,  $A_{ps2}$  required in Stage 2 using an increased lever arm (Elliott 2002). The ratio with the calculated values were more than 1.00, except for

specimen SR1, where the  $\frac{M_{crack\ exp}}{M_{crack\ calc}} = 0.96 \leq 1.00$ . Although the ratio was less than

1.00 but at failure  $\frac{M_{ur\ exp}}{M_{ur\ calc}} = 1.17 \geq 1.00$ . This shows that the ultimate bending moment capacity of specimen SR1 was still 17% higher than  $M_{ur\ calc}$  although the earlier cracking occurred below the expected  $M_{crack\ calc}$ .

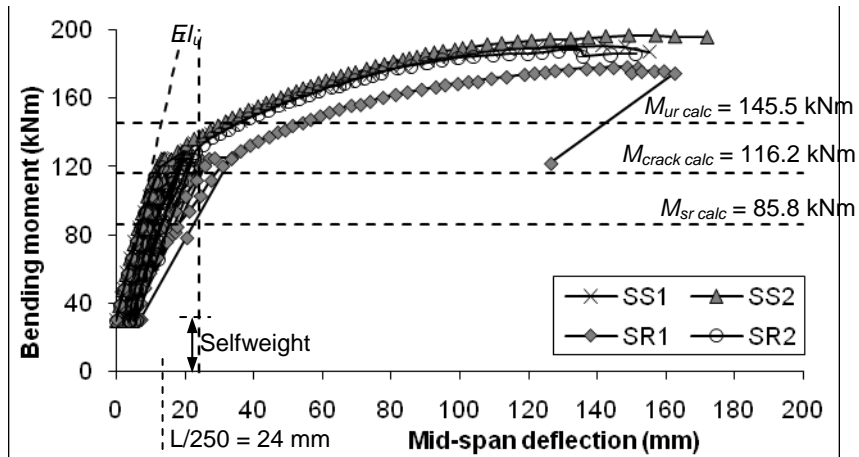


Figure 8 Bending moment vs. mid-span deflection relationship

For all specimens, the first crack occurred at the mid-span. As further loading was applied, more cracking develops in the tension region and moves toward the compression region before crossing the interface into the concrete toppings. The same cracking pattern was observed at both sides for each specimen. Except for specimen SS1, although cracking crossed the interface and into the concrete toppings, there was no failure in the interface (zero slippage). This is shown in Fig. 9 for specimen SR2. For specimen SR1 and SR2, the test was stopped when concrete crushing occurred on the top surface at the mid-span region.

Table 2 Specimen self weight and recovery during the cyclic loading

Specimen	Recovery (%)			First cracking moment, $M_{crack,exp}$ (kNm)	Ultimate moment of resistance, $M_{ur,exp}$ (kNm)	$\frac{M_{crack,exp}}{M_{crack,calc}}$	$\frac{M_{ur,exp}}{M_{ur,calc}}$
	1 <sup>st</sup> Cycle	2 <sup>nd</sup> Cycle	3 <sup>rd</sup> Cycle				
SS1	83.6	83.2	79.1	128.7	190.3	1.15	1.25
SS2	84.1	83.5	78.5	133.2	196.8	1.19	1.29
SR1	81.7	82.0	77.5	107.7	178.2	0.96	1.17
SR2	80.7	81.0	80.8	119.8	188.1	1.07	1.23



Figure 9 Flexural cracking pattern at failure for specimen SR2

### 5.2 Bending Moment and Concrete Strains Relationship

A typical bending moment vs. concrete strains relationship at the top, bottom and interface is shown in Fig. 10 and the strain distribution is shown in Fig. 11. The calculated neutral axis depth shown in the figure from the uncracked,  $x_u$  and cracked,  $x_c$  section were calculated using the following equation:

$$x_u = \frac{A_{hcu}y + A_{top}y + A_s(m - 1)d}{A_{hcu} + A_{top} + A_s(m - 1)} \quad (1)$$

$$x_c = \frac{b_{eff} \frac{x_c^2}{2} + mA_s d}{b_{eff} x_c + mA_s} \quad (2)$$

where  $A_{hcu}$  is the cross sectional area of the hollow core unit,  $A_{top}$  is the cross sectional area of the concrete topping,  $A_s$  is the total reinforcement area,  $y$  is the centroid of the area considered from the point of reference,  $b_{eff}$  is the effective breadth and  $m$  is the steel to concrete modular ratio. For specimen SS1 and SS2, the measured strains were acting elastically until  $M_{crack\ calc}$ . During this behaviour, the difference in the calculated strain,  $EI_u$  was below 10%. After cracking, the specimens behaved non-linearly. When the specimens were close to their ultimate capacity, large bottom strain increments of more than 2000  $\mu\epsilon$  were observed for a small increment of load. Specimens SR1 and SR2 acted non-linearly after the first crack occurred, which was below  $M_{crack\ calc}$ . Beyond this point and up to ultimate, the strains were behaving similarly to specimen SS1 and SS2. The strain distribution changes rapidly when multiple flexural cracks start to occur. At the same time, the interface strain changes from negative (compression) to positive (tension).

At uncracked, the neutral axis was below the interface (in the HCU) and as the section cracked, the neutral axis moved above the interface into the concrete toppings. At failure, the neutral axis (measured from the top of the composite slab) reduced from 102.4

to 33.0 and 49.8 mm for specimen SS1 and SS2, respectively. The same was observed for specimen SR1 and SR2, where the neutral axis reduced to 38.9 and 52.8 mm at failure. The neutral axis reduced considerably for specimen SS1 and SR1, where the surface was ponded. However, the difference was only 3.7% compared to the calculated  $x_c = 34.2$  mm (measured from the top composite slab) suggesting the interface was not disturbed at failure.

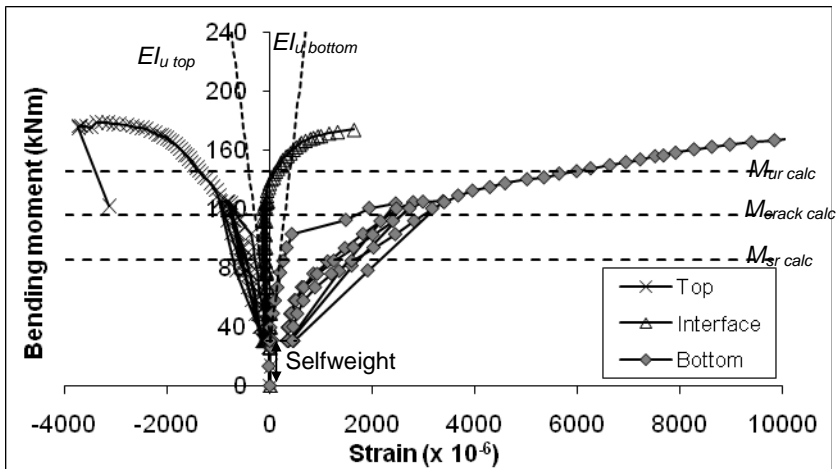


Figure 10 Typical concrete strains relationships for specimen SR1 up to 10000  $\mu\epsilon$

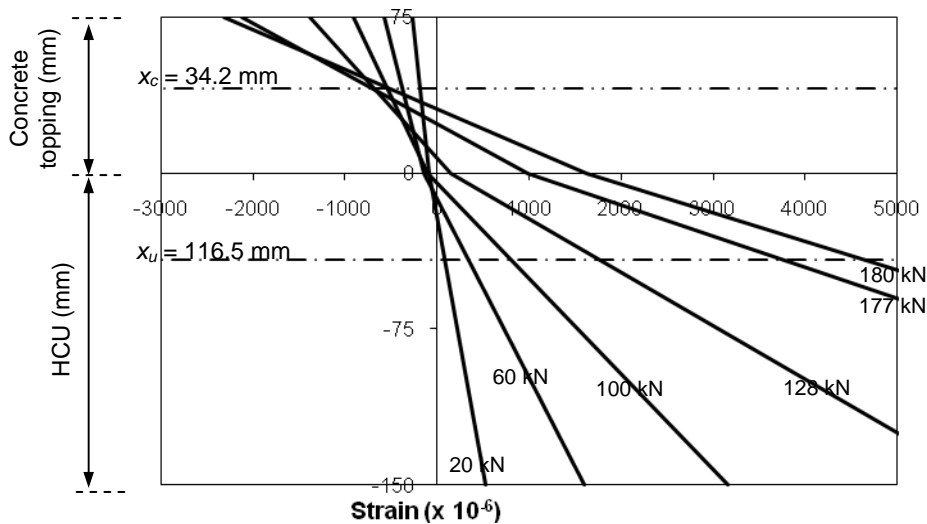


Figure 11 Typical strain distribution diagram for specimen SR1

### 5.3 Surface Roughness and Interface Slip

The roughness profile at the mid-span of each specimen is shown in Fig. 12(a) and 12(b). Higher amplitude can be seen in the rough surface profile showing higher peaks and valleys compared to the smooth surface. In fact, the smooth surface profile seems to show equal heights throughout the whole sample length. Roughness is usually represented as the average roughness,  $R_a$  which is the average value of the departure of the profile above and below the mean lines throughout the sampling length,  $l$  (see Fig. 13(a)). A recent study by Santos et. al. (Santos, Julio et al. 2007) suggested to use other alternatives like the mean peak-to-valley height, total roughness height or maximum valley depth to determine the roughness amplitude, since these correspond to the highest coefficient of correlation obtained. The mean peak-to-valley height,  $R_z$  represents the distance between the five highest profile peaks and the five deepest profile valleys within the sampling length,  $l$  as shown in Fig. 13(b). The definition of  $R_z$  is given as (BSI 1988):

$$R_z = \frac{1}{5} \sum_{i=1}^5 z_i \tag{3}$$

The total roughness height,  $R_y$  is given by (BSI 1988):

$$R_y = p_{max} - v_{max} \tag{4}$$

where  $p_{max}$  is the maximum peak height and  $v_{max}$  is the maximum valley depth.

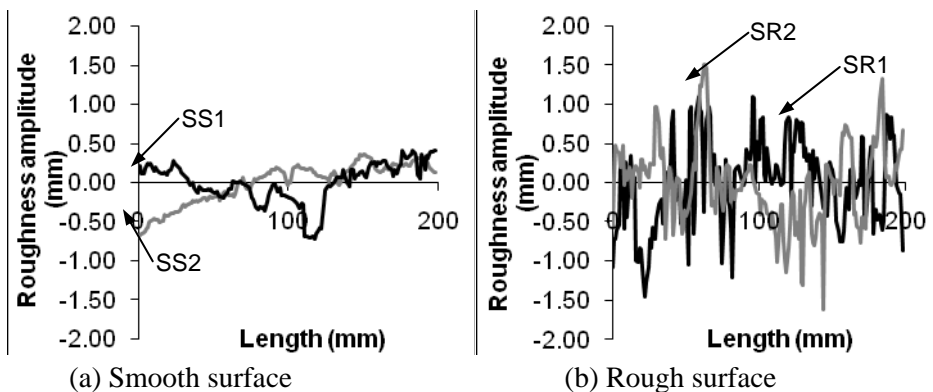


Figure 12 Surface profile measured at the mid-span

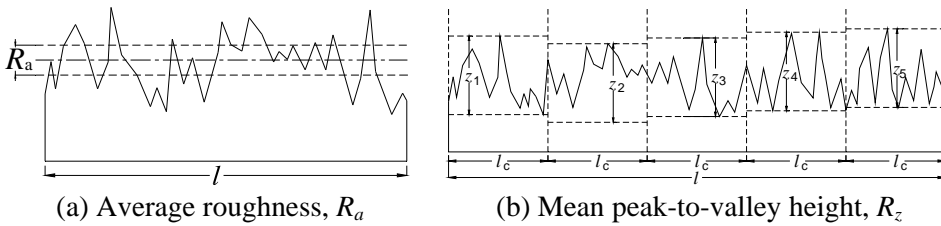


Figure 13 Determination of  $R_a$  and  $R_z$

The values of roughness for the different definition of  $R_a$ ,  $R_z$  and  $R_y$  are given in Table 3. The findings show that when  $R_a$  is considered to define roughness, there was not much difference to differentiate between the smooth and rough surfaces. However, if  $R_z$  and  $R_y$  are considered, the relationship can be divided as follows; (i) smooth surface when  $R_z < 1$  mm and  $R_y < 2$  mm and (ii) rough surface when  $R_z > 1.00$  mm and  $R_y > 2$  mm. In fact, in Gohnert (Gohnert 2000; Gohnert 2003), Santos et. al. (Santos, Julio et al. 2007) and Ibrahim & Elliott (Ibrahim and Elliott 2006) work, they also found that the scatter of data was so broad when  $R_a$  is considered that any trend or correlation is hardly distinguishable. Based on this finding and the suggestion by Santos et. al. (Santos, Julio et al. 2007),  $R_z$  is considered in this study when obtaining the roughness value.

The study found that as roughness increases, the interface slip can be minimised. This was observed during the test where only interface slip occurs in specimen SS1 as shown in Fig. 14. The maximum slip at failure at the left and right position was 0.08 and 0.03 mm, respectively. The slip only occurred for the smooth surface with ponded condition, which was the least roughness values and in contrast to the rough surface (see Table 3). Furthermore, with excessive standing water, the interface is easily disturbed and maybe subjected to slippage. However, by roughening the top surface of the HCU, this will eliminate or reduce any interface slip that may occur. This is observed for specimen SR2 (rough – ponded) where  $R_z = 1.87$  mm compared to 0.51 mm for specimen SS1.

Table 3 Surface roughness results

Specimen	Surface roughness	Surface condition	Average roughness, $R_a$ (mm)	Mean peak-to-valley height, $R_z$ (mm)	Total roughness height, $R_y$ (mm)
SS1	Smooth	Ponded	0.32	0.51	1.60
SS2		Optimum wet	0.25	0.64	1.83
SR1	Rough	Ponded	0.42	1.51	2.92
SR2		Optimum wet	0.48	1.87	3.35

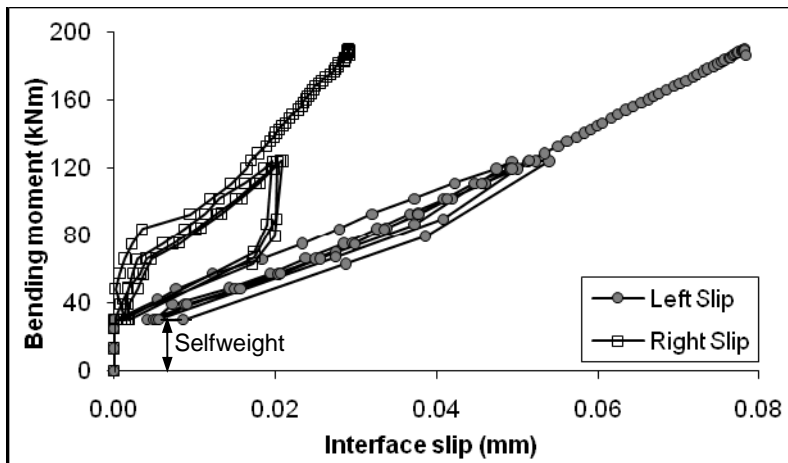


Figure 14 Bending moment vs. interface slip relationship for specimen SS1

### 6.0 Deflection with Partial Interaction

The test results show that interface slip was only observed in specimen SS1. However, for the other specimens with similar strain distribution diagrams pattern shown in Fig. 11, the strain gradients above and below the neutral axis were not the same, suggesting an internal slip occurred in the mid-span region (where the strain gauge was positioned). If this happens, the predicted deflection is based on partial interaction, where the internal interface slip must also be taken into account in the calculation. In 2000, Lam et.al. (Lam, Elliott et al. 2000) proposed a method to predict the deflection with partial interaction. However, the work was on a composite steel beam with precast slabs. The proposed equation was modified in this paper to suit with the type of slab used. The strain distribution from the experimental results and associated with partial interaction is shown in Fig. 15. The shear stiffness,  $K_s$  is given as:

$$K_s = \frac{q l_s}{\delta_s} \tag{5}$$

Where  $q$  is the shear force at the interface per unit length,  $l_s$  is the uniform spacing roughness profile and  $\delta_s$  is the interface slip. Consider a composite slab with axial forces and moments acting on an element shown in Fig. 16. The force and moment for the concrete toppings act through the centroid of the concrete toppings at a distance  $y$ , from the interface, and the force and moment for the HCU act at the centroid of the HCU at a

distance  $y_s$  from the interface. The elastic strain at the bottom of the concrete toppings,  $\epsilon_t$  as shown in Fig. 15 is given as:

$$\epsilon_t = \frac{M_{top} y_t}{E'_c I_{top}} - \frac{F_{top}}{E'_c A_{top}} \tag{6}$$

where  $E'_c$  is the Elastic Modulus of the concrete topping. The elastic strain at the top of the HCU is given by:

$$\epsilon_s = \frac{F_{hcu}}{E_c A_{hcu}} - \frac{M_{hcu} y_s}{E_c I_{hcu}} \tag{7}$$

where  $E_c$  is the Elastic Modulus of the HCU and assuming:

$$F_{int} = F_{top} = F_{hcu} \tag{8}$$

where  $F_{int} = qx$  and the shear force per unit length of the composite slab,  $q$  can be written as:

$$q = \frac{dF_{int}}{dx} \tag{9}$$

Combining Eq. (5) and (9), the interface slip strain in the composite slab,  $\frac{d\delta_s}{dx}$  as shown in Fig. 17, becomes:

$$\frac{d\delta_s}{dx} = \frac{d^2 F_{int}}{dx^2} \frac{I_s}{K_s} = \epsilon_t - \epsilon_s \tag{10}$$

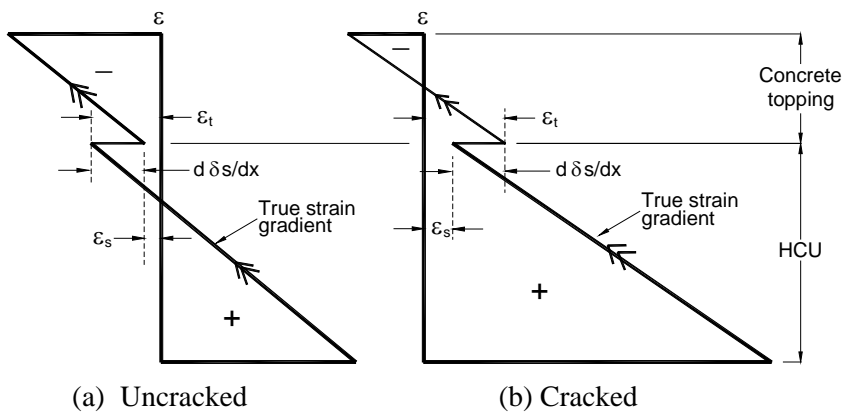


Figure 15 Strain distributions for partial interface interaction

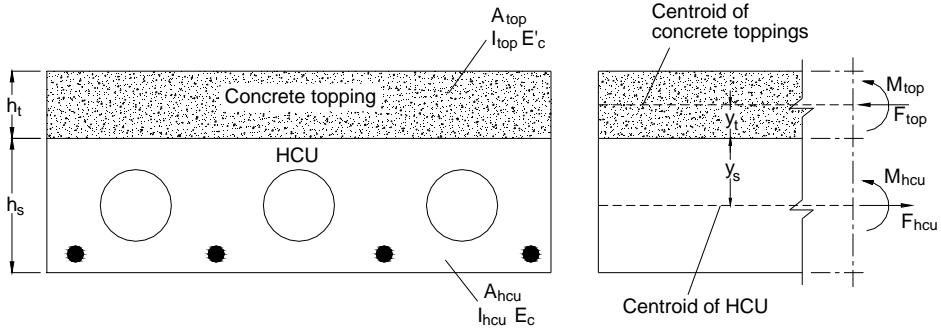


Figure 16 Force and moment distribution of composite slab

When interface slip occurs, the strain diagram can be represented as shown in Fig. 17. In the test setup, electrical strain gauges were positioned at the top and bottom of the HCU and the top surface of the concrete topping as shown in Fig. 6 representing point A, C and D. During the serviceability state and under full-composite action, above and below neutral axis strain gradients are the same as shown in Fig. 17(a). If the interface was disturbed, e.g. interface slip, the strain changed between point B and C. The disturbance to the interface is shown in Fig. 17(b). Therefore, the strain gradient above the neutral axis between point A' and C' was not applicable as it does not represent the actual strain behaviour in the concrete topping, Fig. 17(c). This is known as the “apparent strain gradient”. Therefore, “true strain gradient” can only be determined using the values of point C' and D'. Here, the terms  $(\epsilon_t - \epsilon_s)$  is also the difference between strains at point B' and C',  $\epsilon_{B'C'}$ . Combining Eq. (6), (7), (8) and (10) gives:

$$\frac{I_s}{K_s} \frac{d^2 F_{int}}{dx^2} = \frac{M_{top} y_t}{E'_c I_{top}} + \frac{M_{hcu} y_s}{E_c I_{hcu}} - F_{int} \left( \frac{1}{E'_c A_{top}} + \frac{1}{E_c A_{hcu}} \right) \tag{11}$$

The composite moment,  $M_{comp}$  is equal to:

$$M_{comp} = M_{top} + M_{hcu} + F_{int} (y_t + y_s) \tag{12}$$

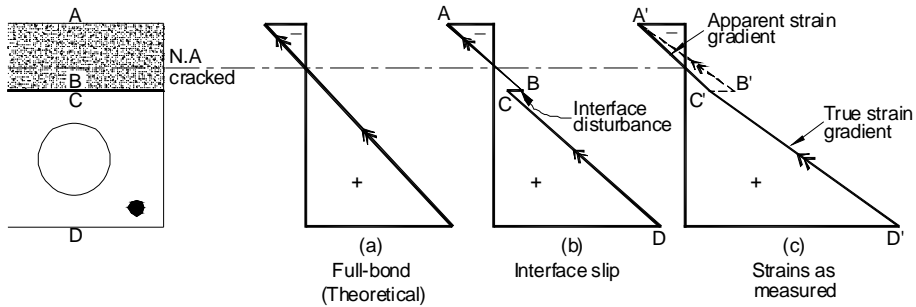


Figure 17 Strain distribution diagram during the ultimate load test

For the composite slab to act monolithically and to prevent any separation between the HCU and concrete toppings, the curvature  $\kappa$  for the concrete toppings and the HCU must be the same, so that:

$$\kappa = \frac{M_{top}}{E'_c I_{top}} = \frac{M_{hcu}}{E_c I_{hcu}} = \frac{d^2 y}{dx^2} \tag{13}$$

Therefore,  $M_{top} = \kappa E'_c I_{top}$  and  $M_{hcu} = \kappa E_c I_{hcu}$  and substitution into Eq. (11) and (12) gives:

$$\frac{I_s}{K_s} \frac{d^2 F_{int}}{dx^2} = \kappa y_t + \kappa y_s - F_{int} \frac{1}{EA} \tag{14}$$

and 
$$\kappa = \frac{M_{comp} - F_{int}(y_t + y_s)}{\Sigma BI} = \frac{d^2 y}{dx^2} \tag{15}$$

where  $\frac{1}{EA} = \frac{1}{E'_c A_{top}} + \frac{1}{E_c A_{hcu}}$  and  $BI = E'_c I_{top} + E_c I_{hcu}$

Combining Eq. (14) and (15) gives:

$$\frac{I_s}{K_s} \frac{d^2 F_{int}}{dx^2} = \frac{M_{comp}(y_t + y_s)}{\Sigma BI} - \frac{F_{int}(y_t + y_s)^2}{\Sigma BI} - \frac{F_{int}}{EA} \tag{16}$$

$$\overline{EI} = \sum EI + \overline{EA}(y_t + y_s)^2$$

Using the parallel axis theorem,

Therefore, 
$$(y_t + y_s)^2 = \frac{\overline{EI} - \sum EI}{\overline{EA}}$$
 (17)

Substituting Eq. (17) into Eq. (16) and rearranging them gives:

$$\frac{l_s}{K_s} \frac{d^2 F_{int}}{dx^2} = \frac{M_{comp}(y_t + y_s)}{\sum EI} - \frac{F_{int} \overline{EI}}{\sum EI \overline{EA}}$$
 (18)

i.e. the interface slip strain is due to the difference between the strain due to the  $M_{comp}$  and  $F_{int}$ . Multiplying each term in Eq. (18) with  $\frac{\overline{EA}(y_t + y_s)}{\overline{EI}}$  gives:

$$\left( \frac{\overline{EA}(y_t + y_s) l_s}{\overline{EI} K_s} \right) \frac{d^2 F_{int}}{dx^2} = \frac{M_{comp}(y_t + y_s)^2 \overline{EA}}{\sum EI \overline{EI}} - \frac{F_{int}(y_t + y_s)}{\sum EI}$$
 (19)

and substituting Eq. (17) gives:

$$\frac{M_{comp} - F_{int}(y_t + y_s)}{\sum EI} = \frac{M_{comp}}{\overline{EI}} - \frac{\overline{EA}(y_t + y_s) d^2 F_{int} l_s}{\overline{EI} dx^2 K_s}$$
 (20)

Substituting Eq. (10) and (18) into Eq. (20), gives:

$$\frac{d^2 y}{dx^2} = \frac{M_{comp}}{\sum EI} + \frac{\overline{EA}}{\overline{EI}} (y_t + y_s) s'_B C'$$
 (21)

For mid-span deflection assuming constant moment along the interface and integrating  $\frac{d^2 y}{dx^2}$  twice with respect to  $x$  gives:

$$\delta_{part} = \delta_{full} + \frac{\overline{EA}}{8\overline{EI}} (y_t + y_s) s'_B C' L^2$$
 (22)

where  $\delta_{part}$  is the deflection of the composite slab with partial interaction  
 $\delta_{full}$  is the deflection of the composite slab with full interaction  
 $\varepsilon_{B'C'}$  is the interface slip strain difference

The difference between the measured and the calculated interface strain is the interface slip strain or the interface disturbance,  $\varepsilon_{B'C'}$ . The calculated interface strain was from the “true strain gradient”, which was then applied for the strain gradient above the neutral axis. The relationships between  $EI$  from the “true strain gradient” and  $\varepsilon_{B'C'}$  for specimen SR2 are shown in Fig. 18.

The mid-span deflection comparison with the experimental results,  $\delta_{full}$  (based on the  $EI_u$  of the composite section) and  $\delta_{part}$  from Eq. (20) is shown in Fig. 19 for specimen SR2. The  $\delta_{part}$  and  $\delta_{exp}$  curves show linear relationship before reaching the cracking moment,  $M_{crack\ calc}$ . However, the deflection for both curves during this stage was 3 to 5% more than the  $\delta_{full}$  curve. The possible explanation of the results is that there was an interface slip occurred near the mid-span region even though cracking was not observed during this stage. After cracking occurred, non-linear behaviour was observed and as the specimen was near to failure, both  $\delta_{part}$  and  $\delta_{exp}$  curves was in agreement showing larger deflection of more than 8 mm per loading increment.

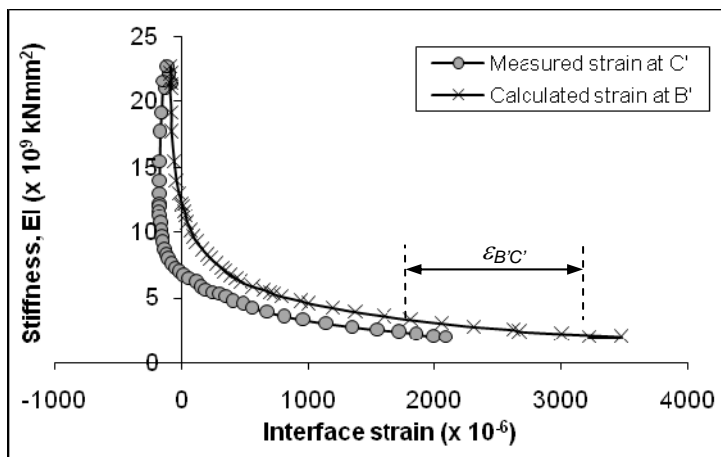


Figure 18 Relationship between stiffness, the measured and calculated interface slip for specimen SR2

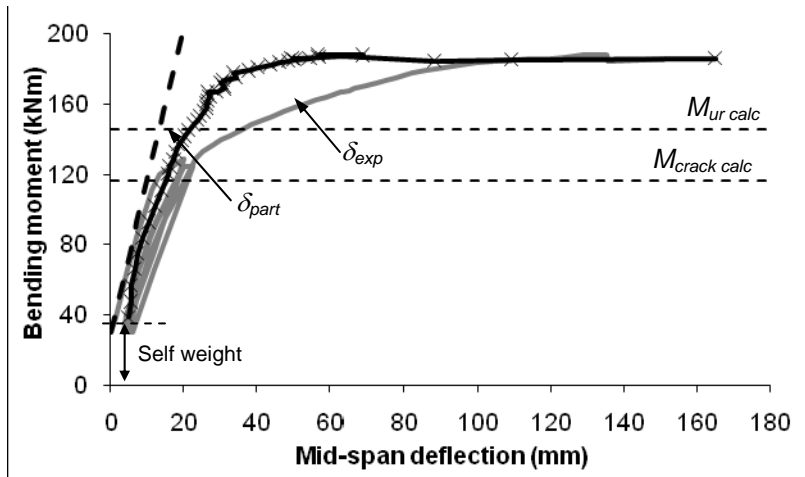


Figure 19 Deflection with partial interface interaction compared to the experimental results for specimen SR2

The relationship between the bending moment and the ratio,  $\eta$ , is shown in Fig. 20, where  $\eta$  is the mid-span deflection ratio with full and partial interaction. If  $\eta = 1.0$ , it is suggested that full composite action was achieved and as  $\eta$  decreases, an interface slip near the mid-span region may have occurred. When this occurred, only partial composite action was achieved and if  $\eta$  reaches zero, full separation at the interface may have occurred. In this study, the figure shows a decrease from 1.0 to 0.08 and 0.03 for all specimens as the bending moment reached its ultimate capacity. However, the worst case was observed for specimens with ponded for both the smooth and rough surfaces. Therefore, the results show obvious influence of surface preparation to the overall performance of the composite slab. The decrease in ratio  $\eta$  shows that  $\delta_{part}$  are higher than  $\delta_{full}$  after  $M_{crack}$  before following the  $\delta_{exp}$  curve.

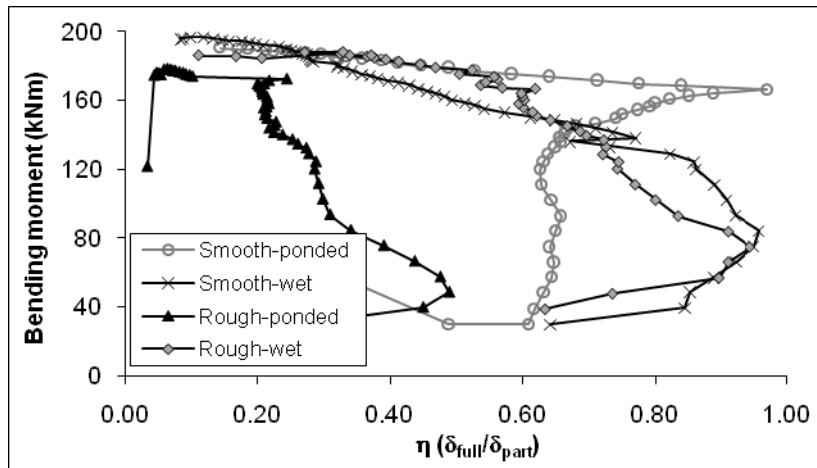


Figure 20 Bending moment vs. the ratio of the full and partial interface interaction

## 7.0 Conclusions

The results and analysis of the bending test carried out in this study can be summarised as follows:

- (a) The ultimate bending moment capacity for the ponded condition for both smooth and rough surfaces was 3 to 5% less than the optimum wet condition.
- (b) The ponded condition specimens for the smooth and rough surfaces showing no reduction to the ultimate bending moment capacity and was 17 to 25% higher than  $M_{ur\ calc}$ .
- (c) Interface slip of 0.08 mm was only observed for the smooth-ponded specimen. It was later found that by roughening the top surface of the HCU, the interface slip can be eliminated.
- (d) A modified theoretical approach to predict the deflection due to partial interaction,  $\delta_{part}$  was proposed in this study as given in Eq. (22) and later compared with the experimental curves of the bending moment – mid-span deflection relationship.
- (e) From the theoretical approach and discussion, the study found that an interface slip may have occurred near the mid-span region although they were not observed by the slip gauge located at both ends of the specimen.

## 8.0 Acknowledgement

This work was funded in part by the Ministry of Higher Education Malaysia (MOHE), Universiti Teknologi Malaysia (UTM) and Precast Flooring Federation (PFF). The author would wish to thank Tarmac Topfloor UK Limited for supply of test components and technical support, and to the technicians in the Department of Civil Engineering, University of Nottingham for their skilled work.

## References

- Ajdkiewicz, A. B., Kliszczewicz, A. T., et al. (2007). Behaviour of Pre-tensioned Hollow Core Slabs with In-situ Concrete Topping. *FIB Symposium: Concrete Structures - Simulators of Development*. Structural Engineering Conferences (SECON), Dubrovnik, 459-466.
- Bensalem, K. (2001). *The Structural Integrity of Precast Concrete Floor Systems Used as Horizontal Diaphragms*. Ph.D Thesis, University of Nottingham, Nottingham.
- British Standard Institute (BSI) (1985) *BS 8110: Part 2: 1985. Structural Use of Concrete - Part 2: Code of Practice for Special Circumstances*. London.
- British Standard Institute (BSI) (1988) *BS 1134: Part 1: 1988. Assessment of Surface Texture - Part 1: Methods and Instrument*. London.
- Elliott, K. S. (2002). *Precast Concrete Structures*. Oxford: Butterworth-Heinemann Publications.
- Federation Internationale de la Precontrainte (FIP) (1982) *FIP Guide to Good Practice - Shear at the Interface of Precast and In-situ Concrete*. Wrexham Springs.
- Girhammar, U. A. and Pajari, M. (2008). Tests and Analysis on Shear Strength of Composite Slabs of Hollow Core Units and Concrete Topping. *Construction and Building Materials*. 22: 1708-1722.
- Gohnert, M. (2000). Proposed Theory to Determine the Horizontal Shear Between Composite Precast and In-situ Concrete. *Cement and Concrete Composites*. 22 (6): 469-476.
- Gohnert, M. (2003). Horizontal Shear Transfer Across a Roughened Surface. *Cement and Concrete Composites*. 25 (3): 379-385.
- Ibrahim, I. S. and Elliott, K. S. (2006). Interface Shear Stress of Hollow Core Slabs with Concrete Toppings. *Sixth International Conference on Concrete Engineering and Technology (CONCET 2006)*. Institution of Engineers Malaysia, Kuala Lumpur, 104-116.
- Lam, D., Elliott, K. S., et al. (2000). Designing Composite Steel Beams with Precast Concrete Hollow-Core Slabs. *Proceedings of the Institution of Civil Engineers: Structures and Buildings*. 140: 139-149.
- Ros, P. S., Cabo, F. D., et al. (1994). Experimental Research on Prestressed Hollow Core Slabs Floors with Insitu Concrete Topping. *FIP 12th International Congress*. Federation Internationale de la Precontrainte, Washington, C33-C41.
- Santos, P. M. D., Julio, E. N. B. S., et al. (2007). Correlation Between Concrete-to-concrete Bond Strength and the Roughness of the Substrate Surface. *Construction and Building Materials*. (21): 1688-1695.
- Scott, N. L. (1973). Performance of Precast Prestressed Hollow Core Slab with Composite Concrete Topping. *PCI Journal*. 18 (2): 64-77.

- Ueda, T. and Stitmannathum, B. (1991). Shear Strength of Precast Prestressed Hollow Slabs with Concrete Topping. *ACI Structural Journal*. 88 (4): 402-410.
- Walraven, J. C. (1991). *Theoretical Aspects of Composite Structures*. Netherlands, University of Technology Delft.